Electronic Supplementary Information

One-pot polymer-clay composite reversible adhesive

Table of contents

Table S1. Solid mass fraction and monomer conversion.

Sample	Solid mass fraction [%]	Monomer conversion [%]
A0	29.3±0.7	98.4±2.3
A25	29.2±0.5	98.0±1.8
A50	29.3±0.4	98.2±1.2
A75	29.2±0.4	97.7±1.5
A100	29.4±0.5	98.2±1.5
A125	29.4±0.5	98.0±1.8
A150	29.4±0.8	97.9±2.8
C0	22.6±0.8	78.9±2.8
C25	23.6±0.5	82.4±1.8
C50	23.6±0.7	81.9±2.4
C75	23.1±1.2	80.0±4.3
CPS25	23.7±1.0	82.1±3.4
CPS50	23.9±0.9	82.6±3.1
CPS75	24.1±1.2	82.5±4.2

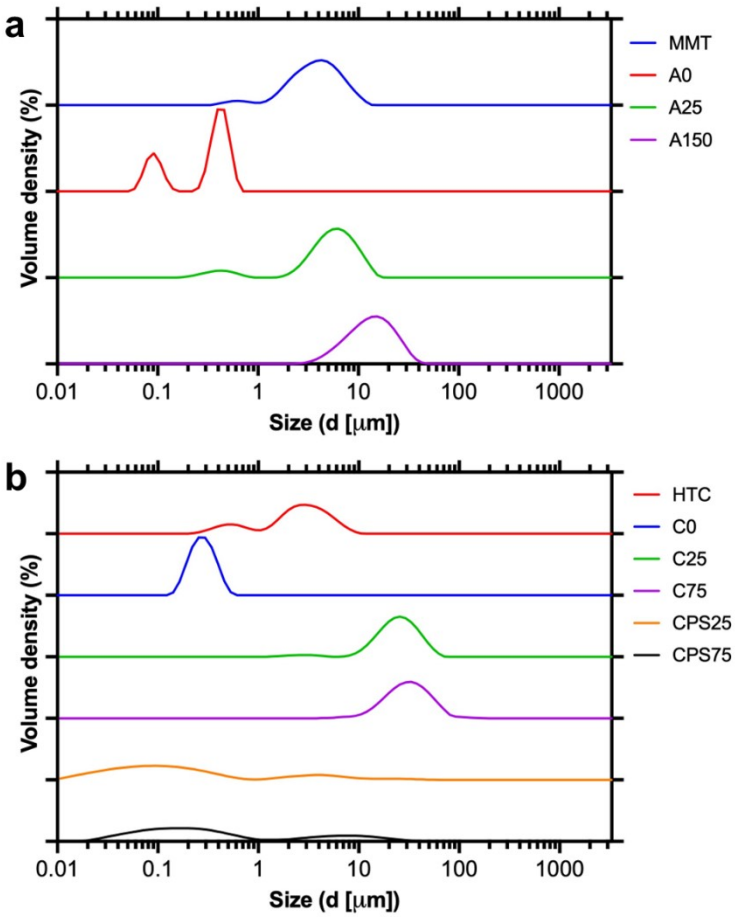

Figure S1. Particle size data for (**a**) P(St-BA)/PAA-MMT, and (**b**) P(St-BA)/Chi-HTC and P(St-BA)/Chi-HTC/PS80 emulsion composites.

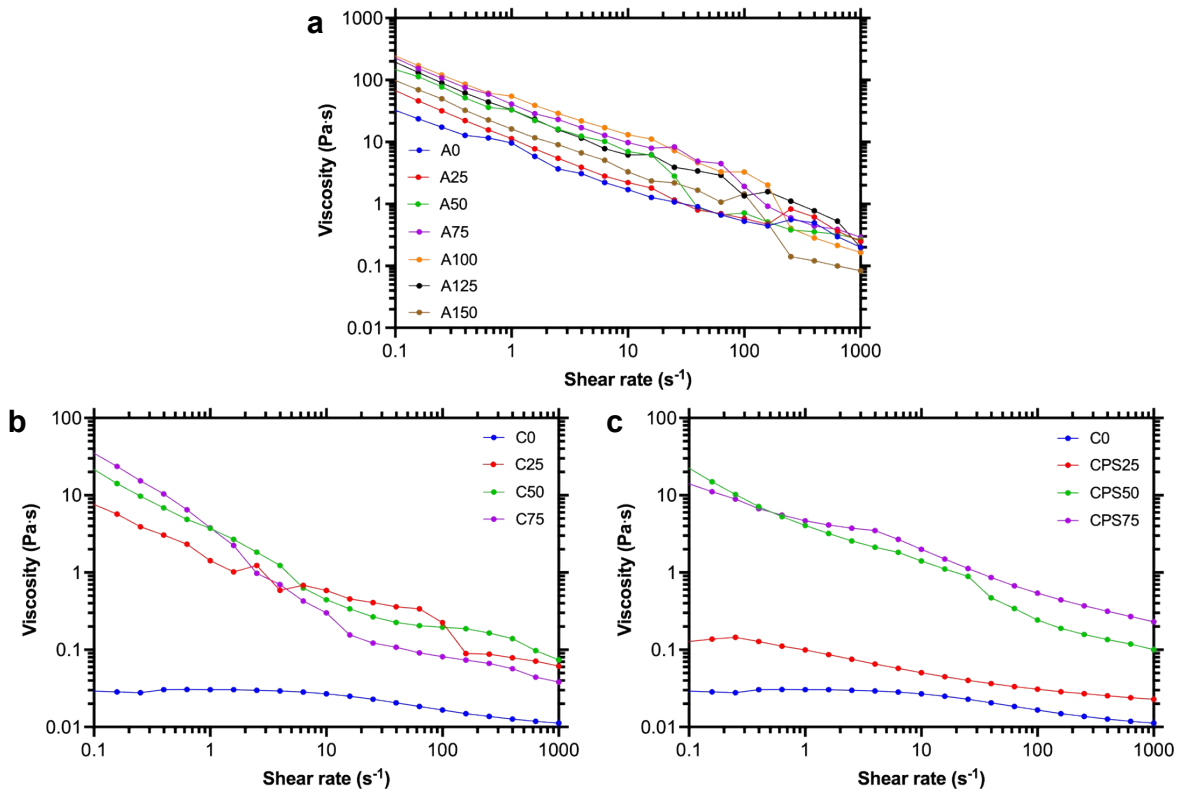

Figure S2. Viscosity of (**a**) P(St-BA)/PAA-MMT, (**b**) P(St-BA)/Chi-HTC, and (**c**) P(St-BA)/Chi-HTC/PS80 emulsion composites as a function of shear rate. Instability at higher shear rates might be due to different physical and interfacial mechanisms including wall slip (e.g., sudden drop in viscosity as in A150), droplet deformation, viscous heating, or sample drying.[1–3]

1 S. R. Derkach, *Adv. Colloid Interface Sci.*, 2009, **151**, 1–23.
2 C. J. Pipe, T. S. Majmudar and G. H. McKinley, *Rheol. Acta*, 2008, **47**, 621–642.
3 P. Lehéricey, P. Snabre, A. Delots, N. Holten-Andersen and T. Divoux, *J. Rheol.*, 2021, **65**, 427–436.

Figure S3. Sagging processes of A0 (left) and A100 (right). A volume of 0.2 mL was used on both cases.

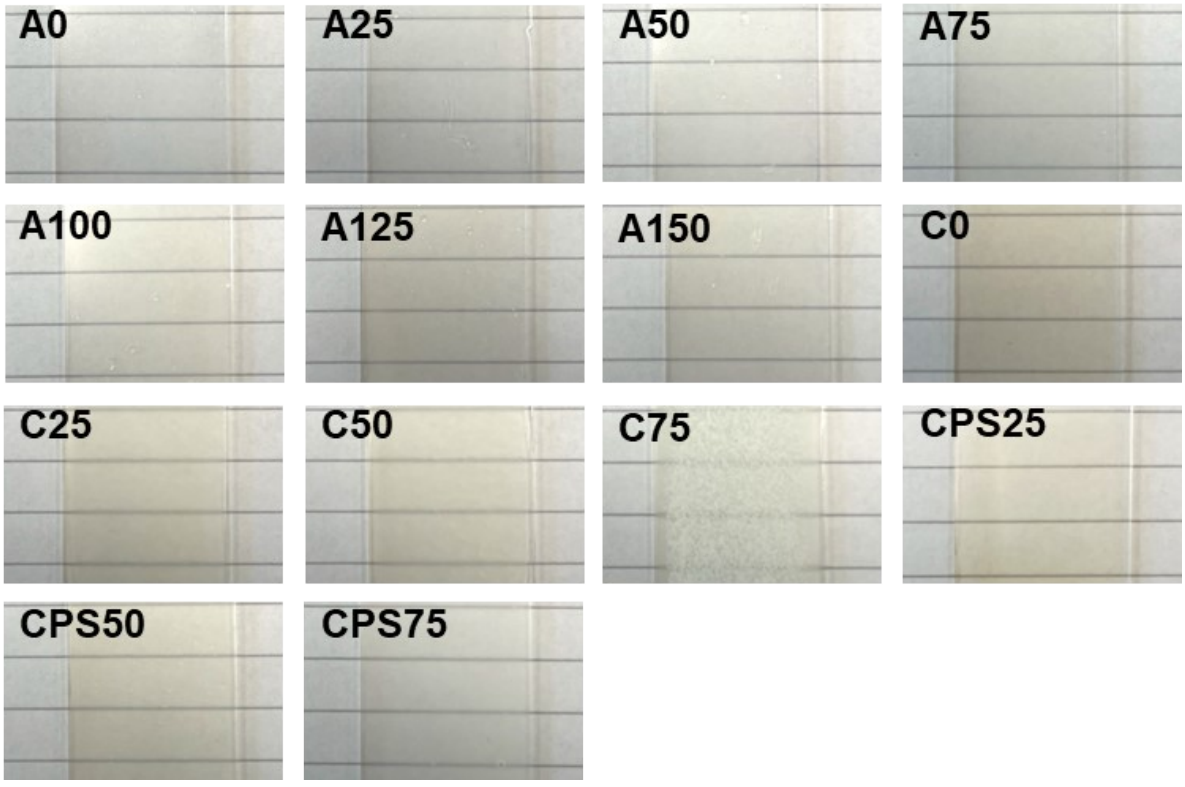

Figure S4. Emulsion composite films on glass. The backdrop is 7 mm ruled paper, and all photographs were taken under the same optical conditions.

Table S2. Water contact angles for emulsion composite films.

Sample	HCl pH 1	Water	NaOH pH 14
A0	34.19	30.32	25.48
A25	32.5	18.5	38.29
A50	30.01	21.35	37.25
A75	26.83	24.85	35.51
A100	22.28	28.17	32.56
A125	26.56	28.02	34.03
A150	32.6	31.82	34.47
C0	76.39	88.66	93.36
C25	86.78	93.82	102.22
C50	91.09	98.5	111.24
C75	123.83	124.38	135.89
CPS25	93.65	94.61	99.18
CPS50	71.85	71.72	87.08
CPS75	64.86	65.03	73.08

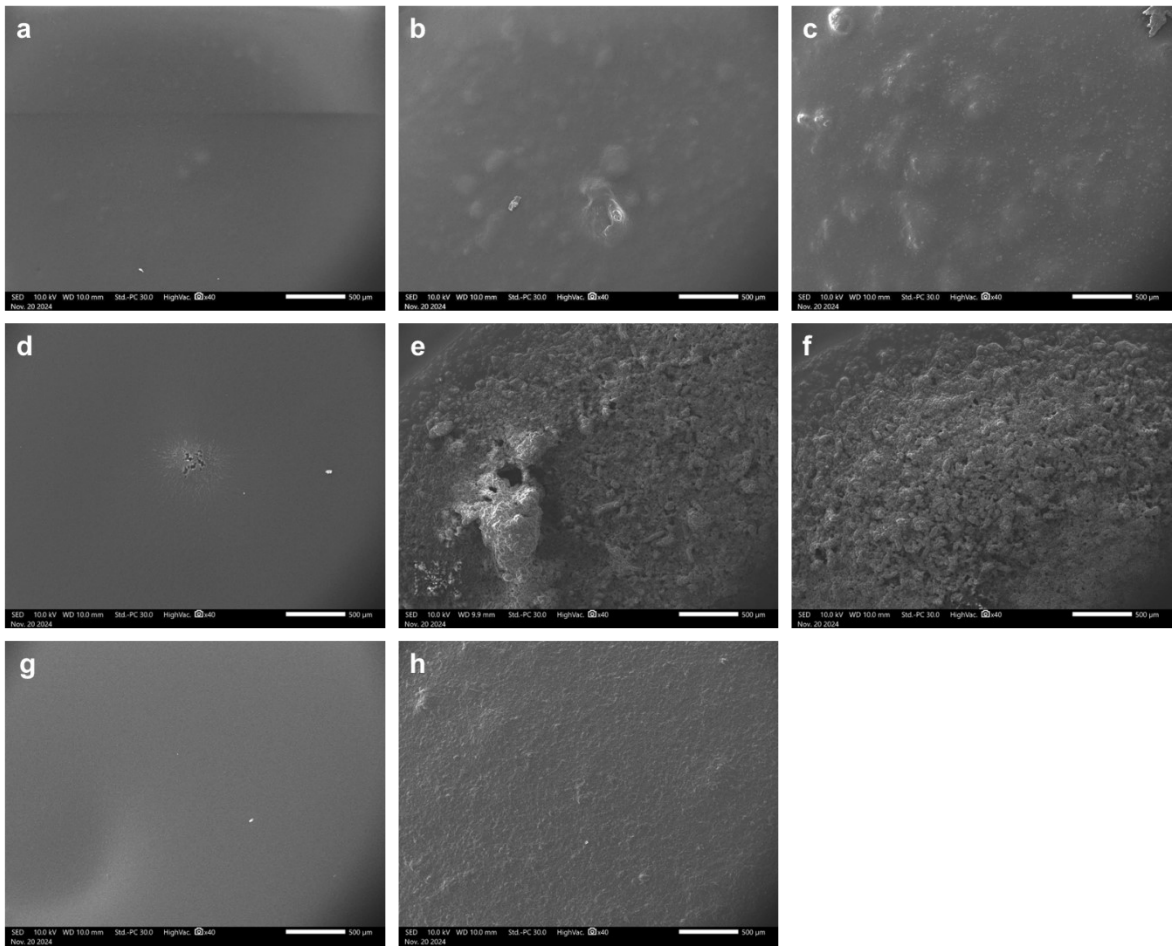

Figure S5. Representative scanning electron microscopy images of (**a**) A0, (**b**) A25, (**c**) A150, (**d**) C0, (**e**) C25, (**f**) C75, (**g**) CPS25, and (**h**) CPS75.

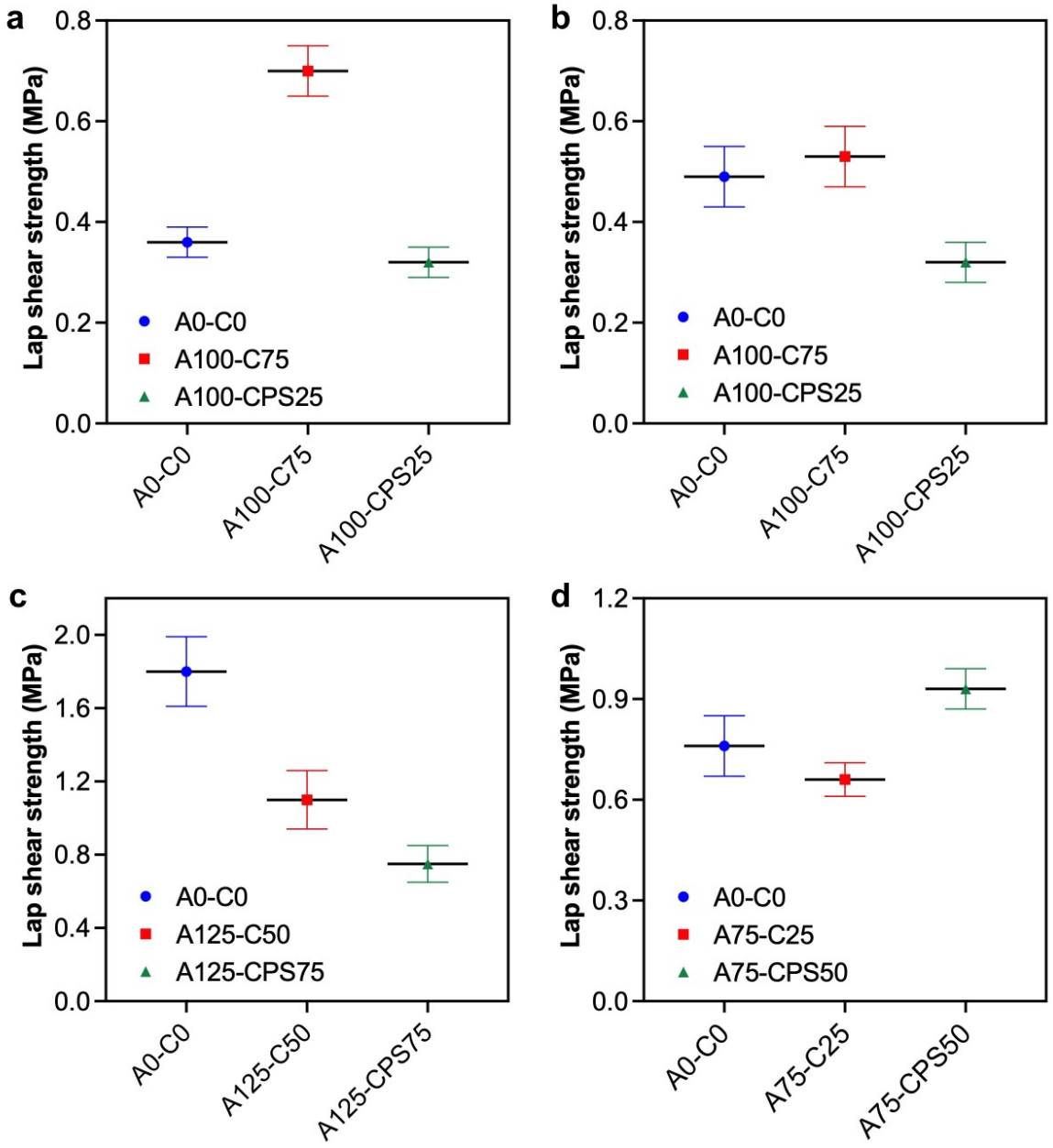

Figure S6. Lap shear test results for representative dual adhesive systems on (**a**) PET, (**b**) PP, (**c**) Al, and (**d**) PC.

Table S3. Reversibility under static conditions. An X indicates no detachment was observed. The time indicates how long it takes for the sample to detach.

PET	PP	pH 1	pH 7	pH 14
A0	A0	X	X	X
A25	A25	X	X	24 h
A50	A50	X	X	24 h
A75	A75	X	X	24 h
A100	A100	X	X	24 h
A125	A125	X	X	24 h
A150	A150	X	X	24 h
C0	C0	X	X	X
C25	C25	48 h	X	X
C50	C50	48 h	X	X
C75	C75	24 h	X	X
CPS25	CPS25	48 h	X	X
CPS50	CPS50	24 h	X	X
CPS75	CPS75	24 h	X	X
C0	A0	48 h	X	48 h
A0	C0	48 h	X	48 h
C75	A100	24 h	X	24 h
A100	C75	24 h	X	24 h
CPS25	A100	24 h	X	24 h
A100	CPS25	24 h	X	24 h

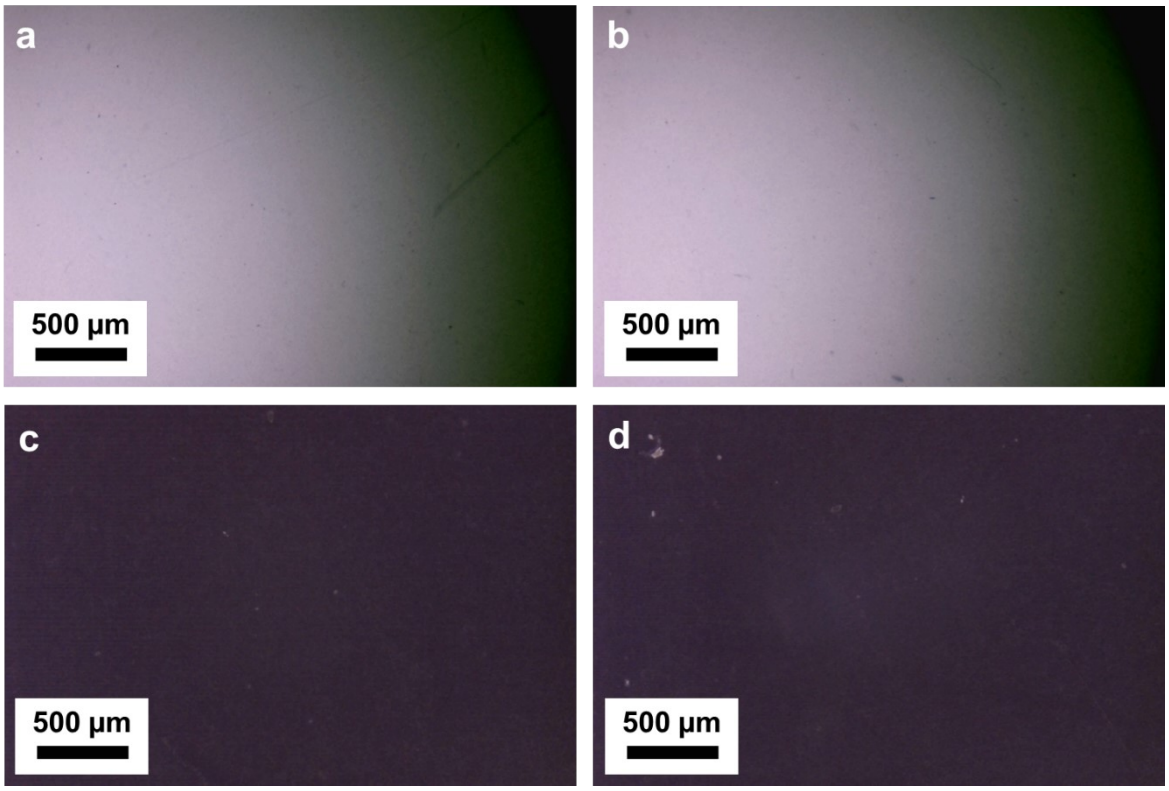

Figure S7. Optical micrographs of substrates: (**a**) as-received PET, (**b**) PET after debonding of sample A100, (**c**) as-received PP, and (**d**) PP after debonding of sample A100.

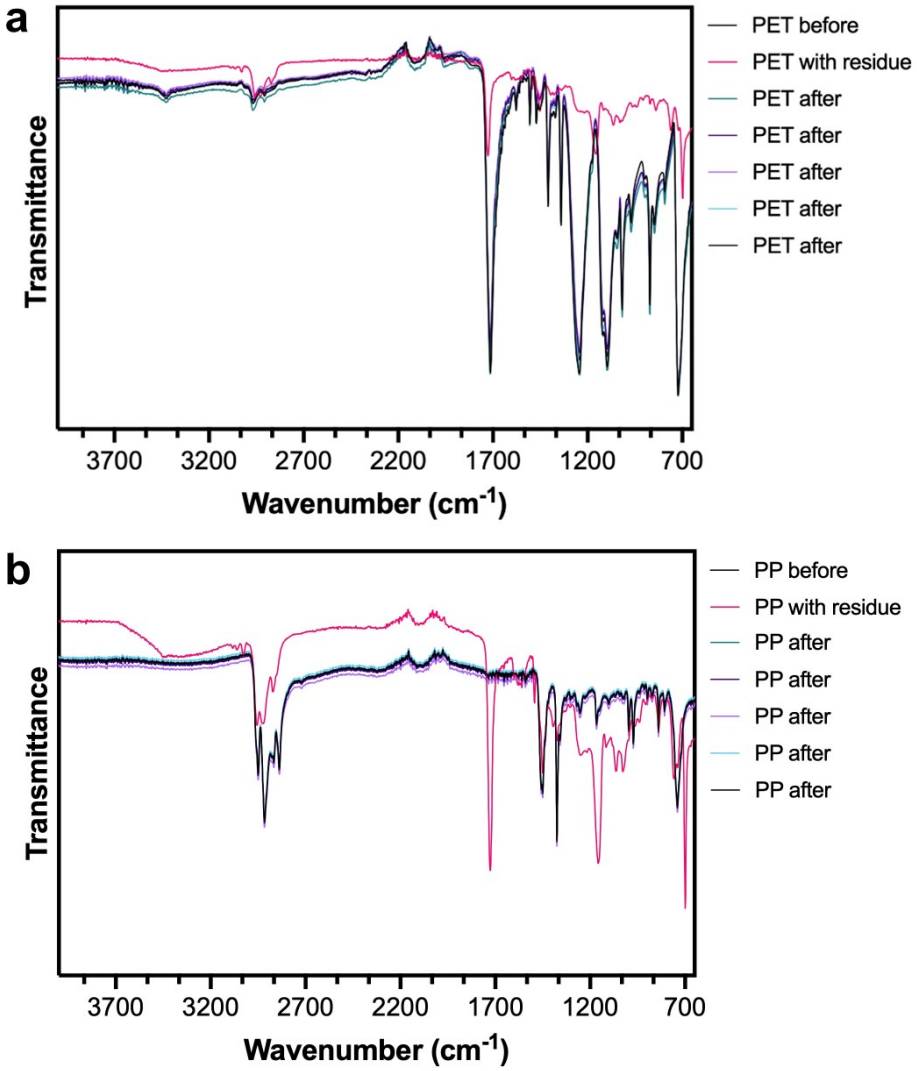

Figure S8. ATR-FTIR spectra of (**a**) PET and (**b**) PP substrates. Data shows plastic films before adhesion with the A100 formulation, at five random locations after detachment in alkaline solution, and where adhesive residue was observed due to mechanical failure.

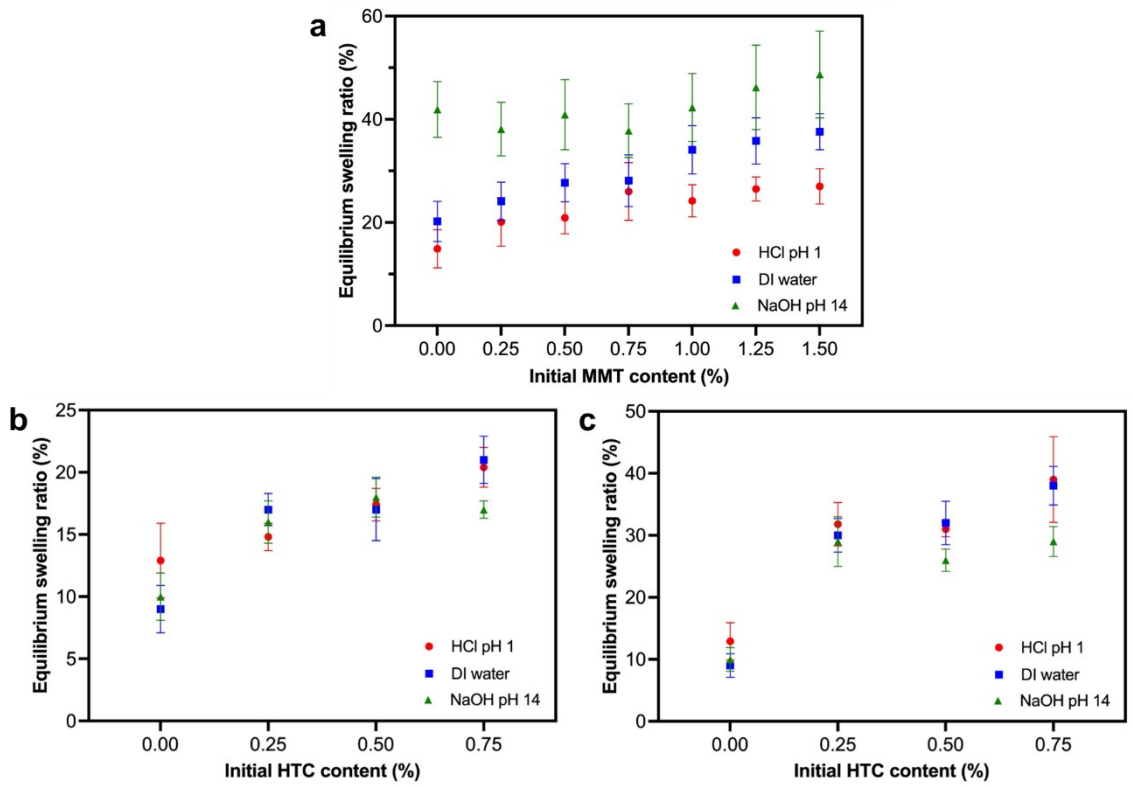

Figure S9. Equilibrium swelling percentages of (**a**) P(St-BA)/PAA-MMT, (**b**) P(St-BA)/Chi-HTC, and (**c**) P(St-BA)/Chi-HTC/PS80 emulsion composite films.